Functional MRI Using Super-Resolved Spatiotemporal Encoding

Noam Ben-Eliezer[1], **Ute Goerke**[2], **Kamil Ugurbil**[2], and **Lucio Frydman**[1]

[1]Chemical Physics Department, Weizmann Institute of Science, 76100 Rehovot, Israel

[2]Center for Magnetic Resonance Research and Department of Radiology, University of Minnesota Medical School, Minneapolis, Minnesota

Abstract

Recently, new ultrafast imaging sequences such as RASER and Hybrid SPEN MRI have been proposed, in which the phase-encoding of conventional Echo Planar Imaging (EPI) is replaced with a spatiotemporal-encoding (SPEN). In contrast to EPI, SPEN provides significantly higher immunity to frequency heterogeneities including those caused by B_0-inhomogeneities and chemical-shift offsets. Utilizing the inherent robustness of SPEN, it was previously shown that RASER can be used to successfully perform fMRI experiments in the orbitofrontal cortex – a task which is challenging using EPI due to strong magnetic susceptibility variation near the air-filled sinuses. Despite this superior performance, systematic analyses have shown that in its initial implementation, the use of SPEN was penalized by lower SNR and higher RF power deposition as compared to EPI-based methods. A recently developed reconstruction algorithm based on super-resolution principles, is able to alleviate both of these shortcomings; the use of this algorithm is hereby explored within a functional MRI context. Specifically, a series of fMRI measurements on the human visual cortex, confirmed that the super-resolution algorithm retains the statistical significance of the BOLD response, while significantly reducing the power deposition associated with SPEN, and restoring the SNR to levels that are comparable with those of EPI.

Keywords

functional MRI; spatiotemporal encoding; super-resolved processing; high-field MRI; visual BOLD activation

INTRODUCTION[1]

Functional magnetic resonance imaging (**fMRI**) is one of the most commonly used tools for studying brain cognition and function. The physiological basis of this non-invasive method relies on local changes in neural activity, which instigates transient increases in vascular blood oxygenation, blood volume and blood flow (i.e., the BOLD effect). These in turn can be probed using T_2 and T_2^*-weighted single-shot multidimensional MR imaging methods

Corresponding author: Prof. Lucio Frydman, Telephone: +972-8-9344903, Fax: +972-8-9344123, lucio.frydman@weizmann.ac.il.

[1]**Abbreviations:** T_1/T_2: longitudinal/transverse spin relaxation time; TR, Repetition Time; SNR, Signal to Noise Ratio; EPI, Echo Planar Imaging; GE, Gradient-Echo; SE, Spin-Echo; RASER, Rapid Acquisition by Sequential Excitation and Refocusing; ROI, Region of Interest; FT, Fourier Transform; PSF, Point-Spread Function characterizing the spatial resolution; SPEN, SPatiotemporal-ENcoding; RF, Radiofrequency; SR, Super Resolution; *R*-value, RF pulse time-bandwidth product value.

[1–3]. Typically, the Echo Planar Imaging (**EPI**) sequence is used for fMRI experiments, owing its ability to sample transient signal changes with high temporal resolution. EPI images, however, are often prone to signal losses and to severe distortions due to the high sensitivity of this technique to frequency off-resonance artifacts, caused primarily by susceptibility variations or by the presence of multiple chemical species. Particularly challenging is the scanning of brain regions that are close to air-filled cavities such as the orbitofrontal cortex, areas surrounding the ear canals, and the base of the brain, where the acquisition of reliable fMRI data is usually unfeasible. While many techniques have been designed to compensate for such artifacts, these typically involve tradeoffs such as longer overall acquisition times (as in the case of partial or segmented k-space acquisitions), the need for careful pre-calibration (as for z-shim based methods), or the use of post-processing approaches requiring *a priori* knowledge of the B_0 field distribution [4–6]. Other techniques, such as parallel imaging, are also effective in alleviating these artifacts to some extent, yet might introduce reconstruction noise, and do not completely resolve the problems at highly inhomogeneous brain regions such as mentioned above [7,8].

As an alternative to EPI, novel single-shot imaging sequences based on spatiotemporal encoding (**SPEN**) principles have lately been proposed [9,10]. This encoding approach relies on applying a frequency-swept radiofrequency (chirped RF) excitation pulse in the presence of a magnetic field gradient, which acts to spread out the effective resonance frequencies of the spins throughout the region-of-interest (ROI). Acquisition of the spins' response in the presence of a second field gradient then produces a signal $S(t)$, which at each instant in time, is directly proportional to the spin density profile at consecutive points along the encoded axis. As a result no Fourier Transform (**FT**) needs to be involved in the data-processing procedure, and the spin density profile (i.e., the image) can be reconstructed by taking the signal's magnitude: $\rho(\vec{r})\mu\,|S(t)|$. The two single-shot 2D imaging methods that are used in this report, RASER and Hybrid SPEN, incorporate this type of encoding by replacing the blipped phase-encoding of conventional EPI, by a spatiotemporal-encoding. As was previously shown in [11,12], these SPEN-based versions of single-shot MRI provide much higher robustness to magnetic field inhomogeneities as compared to EPI due to a number of reasons. On one hand, SPEN's progressive excitation/acquisition procedures is able to completely refocus spurious spin dephasings throughout the entire acquisition process, thereby producing images that are free of T_2^* relaxation effects, and hence purely T_2-weighted. Analogous refocusing can also be performed in EPI using a spin-echo pulse; this option, however, is less efficient than its SPEN counterpart, as it produces only a single point of refocusing – usually at the k-space center – while leaving a residual T_2^* weighting towards its edges. In addition, the phase-encoding dimension in EPI is highly sensitive to off-resonance frequency offsets, causing phase errors to accumulate over time. This weakness is especially severe in EPI due to the limited bandwidth and long echo times, characterizing this type of sequence [13]. Replacing this phase-encoding with SPEN alleviates these offset and susceptibility problems, owing to the higher gradient amplitudes (and hence higher bandwidths) that the latter method can employ. Similar arguments also explain SPEN's robustness against multiple chemical shift distortions, vis-à-vis their effect on EPI's low-bandwidth dimension. By utilizing these unique characteristics, the SPEN-based imaging technique RASER, has been used to robustly detect functional activity in the human orbitofrontal cortex at 7 T, and in close proximity to electrophysiological electrodes recording seizures in an animal model of epilepsy [14,15]. In both of these studies, EPI images showed severe morphological distortions and insufficient statistical significance of functional activation.

One of the essential differences between k-space and spatiotemporal-encoding relates to the fact that, whereas the former method encodes the image during the acquisition stage, SPEN encoding is *de-facto* performed during the excitation. SPEN's point-spread-function (**PSF**)

therefore depends on the time-bandwidth product (***R-value***) of the chirp-pulse that is used for exciting the targeted ROI. Subsequently, SPEN's nominal image resolution is proportional to the ratio $ROI/\sqrt{R}$, implying that in order to generate an improved PSF, excitation pulses that have higher *R*-values will be needed. These can be achieved by either increasing the pulse's duration, or by applying the encoding pulse over larger sweep bandwidths [9–11]. Either of these conditions will lead to increased RF deposition and therefore higher specific absorption rate (**SAR**) levels [12]. An additional shortcoming of SPEN is the lower signal-to-noise ratio (**SNR**) that this imaging mode will deliver compared to EPI [14,16]. This can in turn be traced to SPEN's reliance on non-Fourier-based procedures, which deprive this technique from the multiplexing advantage that is inherent in the Fourier transform (i.e., Fellget's advantage).

In a recent report, we presented an approach whereby these SNR and SAR drawbacks can be overcome using a novel image reconstruction algorithm based on super-resolution (**SR**) principles [16]. This form of reconstruction enables one to use excitation pulses that have low bandwidths, and hence low RF power depositions, without compromises on the image quality. In practice, such RF pulses would have lower *R*-values, and relatively broader PSFs, leading to an initially poor spatial localization that is reflected by an overlap between adjacent image pixels. The SR reconstruction can then be used to deconvolve this overlap, and restore the original image resolution. The resolution improvement is performed by replacing the magnitude-mode calculation originally used to process SPEN images, with a least square minimization approach that jointly processes multiple signal points along the SPEN axis for the reconstruction of each image point. As was shown in [16] and further corroborated in [17], this procedure performs very stably under a wide range of imaging conditions, and can provide a reliable single-shot reconstruction of human and animal images *in-vivo*. A second advantage ensuing from the use of SR reconstruction is the ability to compensate for the relatively lower SNR that was initially associated with the magnitude-mode reconstruction of SPEN images. SR achieves this signal enhancement by allowing the use of broader PSFs that effectively sample several pixels at each instant during the acquisition, thereby reinstating to a significant degree the multiplexing advantage of simultaneously processing multiple signal points.

In this Report we investigate the feasibility and prospects of using the super-resolution reconstruction technique for the post-processing of functional MRI data. In order to assess these features, we statistically analyzed the influence of the SR reconstruction algorithm on fMRI data sets collected using SPEN-based sequences, and compared the ensuing results with the output of conventional Gradient Echo EPI (**GE-EPI**) and Spin Echo EPI (**SE-EPI**) sequences.

METHODS

A total of 7 volunteers, ages 20–45, participated in this fMRI study after signing a written consent. Experiments were performed on a 3 T Siemens scanner equipped with a four-channels birdcage coil. Ten blocks of 30 sec left and 30 sec right visual hemifield stimulation using a half circular shifting checkerboard pattern and consisting of black and white concentric rings, were used. Time series of single oblique slices along the calcarine sulcus (marking the location of the primary visual cortex) were acquired in all these fMRI scans. fMRI experiments were performed using the set of pulse sequences shown in Figure 1 including a Gradient-Echo EPI, Spin-Echo EPI and two SPEN schemes: RASER [11] and Hybrid SPEN [16]. In the SPEN experiments (Figures 1c–d), spatiotemporal-encoding was implemented along the vertical y-axis. The spins were excited sequentially in time by applying a magnetic field gradient, and sweeping over the resulting frequency isochromats using a chirped RF pulse [9,18]. The excited isochromats were then refocused using a slice-

selective 180° pulse, and their responses acquired sequentially in time in the presence of an additional gradient. The quadratic phase profile $\varphi_{exc}(y)$ that is inherent to carrying out the excitation with a chirped pulse [19–20] is used to locally probe only the signal near a particular spatial position, thereby obviating the need for a FT along this dimension. The spatial resolution along the SPEN axis is in this case determined by the curvature of the quadratic phase profile at the vertex point (i.e, $^2\varphi_{exc} y^2$) [10]. The readout dimension in all these 2D sequences used a conventional k-space frequency encoding along the x-axis, and was hence reconstructed using standard 1D FT-processing along this axis. In the EPI-sequences, navigator-echoes were used to phase-correct shifts of even and odd echoes of the images [21]. Fat suppression was also implemented in the EPI experiments; no such suppression was required when employing the spatiotemporal-encoding, due to the lack of image artifacts related to resonance frequency offsets in these sequences. Unless otherwise noted, the following imaging parameters were used: matrix size=48×64, slice-thickness=5mm, bandwidth=2004 Hz/pixel, TR=2 sec and TE=30 ms for GE-EPI, and 87 ms for SE-EPI and RASER. In Hybrid SPEN, the echo time TE varied along the spatiotemporally-encoded dimension since the isochromats excited first were acquired last and vice versa. The TE therefore ranged in this case from 69 to 105 ms along the SPEN-encoded dimension; the ensuing implications of this feature are detailed in the Discussion.

In order to evaluate the consequences of using the super-resolution reconstruction algorithm as part of the fMRI data processing procedure, two sets of experiments were performed. The first set consisted of four separate fMRI studies based, respectively, on the GE-EPI, SE-EPI, RASER and Hybrid SPEN sequences. These were all conducted on each of four subjects. The two SPEN sequences were carried out using low RF R-values and were reconstructed using SR. In a second set of experiments, carried out on three volunteers, fMRI data sets were acquired with the RASER and with the Hybrid SPEN sequences – each using both high and low R-values, entailing a total of four separate experimental sessions. These dual R-valued sets were processed, respectively, using a standard magnitude reconstruction of the data (for the high R-value data sets), and using the SR algorithm (for the low R-value data sets) and then compared to each other.

fMRI time-series post-processing

To accommodate for the relatively low gradient slew-rates available in the Siemens scanner used in this study, our implementation employed a constant –rather than a blipped–gradient encoding scheme to progress the acquisition along the SPEN dimension, both for the RASER and for the Hybrid SPEN variants. This resulted in the accumulation of a residual phase shift during the acquisition of even and odd readout echoes. These continuous profile displacements were hence corrected during an initial post-processing stage, using a linear phase correction along the read-out dimension [11]. This procedure, as well as all other data postprocessing procedures, including the super-resolution reconstruction, were implemented using custom-written MATLAB® software packages (The MathWorks, Inc., Natick, MA) and are available upon request.

Following the image's reconstruction, all acquired data were subjected to temporal detrending based on zeroing the mean variance of each time series. Activation maps were then computed using the STIMULATE software package [22], based on statistical t-test of the fMRI time series. No additional processing procedures, such as spatial-smoothing, motion-correction, slice time encoding, and compensation for scanner related temporal instabilities [23] were employed. Since no group average of the activation maps was calculated, conversion of the data to standard space was unnecessary and therefore avoided. In order to improve image quality in the figures, all displayed images were interpolated using STIMULATE. For the statistical analysis of the second study (comparing the use of low, and of high R-values) a reference ROI in the primary visual cortex was automatically

generated for each of the functional maps, based on all activated voxels above a predefined *t*-score threshold. The image SNR for each acquisition and reconstruction approach was then calculated by dividing the signal intensity of this reference ROI, by the standard deviation of the noise at a separate region-of-interest outside the skull where no signal is detected. Further averaging was done over all voxels within the reference ROIs. Statistical analyses of the ten stimulation blocks was then used to compute the mean *t*-score, the number of activated voxels, and the mean image SNR for each subject's reference ROI. The absolute value of the resulting *t*-scores from the left visual stimulation and from the right visual stimulation were consequently combined and averaged over all subjects. Error estimates, representing the standard deviation of the variability between subjects, were also calculated and are reported in Table 1 and in Figure 4 (*vide infra*).

RESULTS

Figure 2 illustrates a representative assessment on the quality of activation maps generated by the super-resolved SPEN MRI approach in comparison with the *k*-space based fMRI imaging sequences depicted in Figure 1. For all subjects and sequences significant activation was found in the left and right visual cortex corresponding to right and left visual hemifield stimulation respectively. The activation followed the gray matter band in all images obtained from SPEN-encoded data sets. Similar activation patterns were obtained from the EPI time series, and from the SPEN data sets reconstructed using the SR algorithm. Consistent with previously published results [14], higher *t*-scores and larger activated regions are visible in the EPI-based imaging methods compared to the maps computed from SPEN based time-series. We attribute these differences to the complete cancellation of the T_2^* relaxation effects in the two SPEN sequences, as compared to the full T_2^*-weighting arising in GE-EPI, and to the residual T_2^*-weighting present in the SE-EPI echo envelop. Considering that this type of relaxation constitutes a major source of BOLD contrast, the maximal *t*-scores and the activated regions can be expected to be larger in T_2^*-weighted sequences than for purely T_2-weighted sequences. SPEN based sequences thus seem to unravel an activation-contrast-mechanism that is predominantly modulated by molecular diffusion [24–31]. Contrary to T_2^*–derived relaxation effects which originate from extravascular magnetic field gradients near capillaries as well as around larger venules, this diffusion-induced modulation of the T_2-contrast is actually higher near small venules and capillaries, and therefore assumed to probe signal changes that are more localized to the actual site of neural activity [32].

In order to quantify the impact of the super-resolution processing on the statistical significance of the BOLD response, a second set of experiments was performed. The ensuing results are summarized in Figure 3, comparing three SPEN images (panels a–c) and three corresponding activation maps (panels d–f) acquired along the calcarine sulcus of one subject using high and low *R*-valued excitation pulses, while maintaining the same spatial resolution. The positive *t*-scores represent stimulation of the left visual hemifield, while the negative values correspond to right visual hemifield stimulation. Reconstruction of these data sets involved a standard FT along the k_x-axis in all images, followed by either application of the SR algorithm for the low *R*-value cases, or by taking the data matrix magnitude for the high *R*-value cases. For all subjects, activation regions in the primary visual cortex –corresponding to the contralateral hemisphere of the presented half-circle visual stimulation– were successfully detected with all imaging protocols and post-processing methods. As a reference, the raw image and functional map from the low *R*-value data sets (right panels) are replicated in the middle panels (3b & 3e), prior to the application of the super-resolution algorithm. Comparison of the middle and right panels validates the ability of the SR algorithm to deconvolve the blurring that emerges at the edges of the brain and within the cluster of activated voxels as a result of the broadened PSF, and to resolve the

image's anatomical features. Note, however, that the data set shown in the middle and right panels was acquired using an excitation pulse having a four times lower R-value, hence depositing four times less RF power, than its counterpart in panels 3a and 3d.

The statistical differences between activation maps originating from the use of high and of low R-values, Figures 3d and 3f respectively, were quantified for a reference ROI in the primary visual cortex. The corresponding results are summarized in Table 1. The most prominent feature arising from this comparison, is that the image's SNR is improved by a factor of 3.5–4 upon using super-resolution vis-à-vis the use of the standard magnitude reconstruction (i.e., for two sets of experiments, producing equivalent spatial resolutions). This increase in SNR holds for both the Hybrid SPEN and for RASER-based sequences, and reflects the reintroduction of the multiplexing advantage brought about into SPEN by SR owing to the broader sampling PSFs, and to its use of a range of consecutive signal points for the reconstruction of each image point [16]. The extent of this advantage is, in practice, predetermined by the RF time-bandwidth product, *i.e.* by the R-value, which affects the intrinsic width of SPEN's sampling PSF [9–11]. As mentioned above the shape of this function relates to the quadratic phase profile produced by the frequency-swept excitation pulse: using high R-values leads to narrow PSFs having nominal widths down to one voxel, while lower R-values produce broader PSFs covering regions that are several voxels wide. These are deconvolved by the SR algorithm, which restores the spatial resolution via the combined processing of multiple signal points arising from overlapping quadratic profiles [16]. Furthermore, since in the high R-value cases the SPEN PSF deviates from an ideal boxcar function, a significant fraction of the theoretically available information is lost in the ramps of these PSFs when processed using simple magnitude reconstruction [11].

Another notable finding emerging from these results is that the difference in the functional contrast, before and after applying the super-resolution procedure, is negligible (Table 1). This observation is consistent with the fact that the reconstruction is performed with an analytical description of the quadratic phase profile, and hence introduces a minimal level of residual noise. Figure 4 further analyzes this aspect by displaying trial averages produced from magnitude and from SR-reconstructions, exemplified for the Hybrid SPEN sequence. The behavior of the trial averages obtained with low R-values, pre- and post-SR processing, were similar within the natural variability of different fMRI scans (cyan and black lines). The relative signal change for time courses reconstructed with super-resolution algorithm is larger than the one obtained with magnitude reconstruction, owing mainly to the better-defined PSFs resulting upon using the SR approach. In addition, since lower gradient strengths are used for SPEN when relying on super-resolution reconstruction, smaller blood-flow-related losses would take place resulting in a larger relative signal change compared to time series acquired with a high R-value.

The statistical significance of the activation pattern in the visual cortex was further quantified by counting the number of activated voxels and calculating the mean t-scores associated with the different imaging and post-processing techniques (Table 1). A small and not significant increase (for a confidence interval of 95%) in the number of activated voxels was observed in the post-SR low R-value case, indicating that the average t-score is not biased by the fraction of activated voxels in the region-of-interest used for the statistical analysis. An increase in the mean t-score, however, was evident upon comparing the average values from the super-resolved Hybrid SPEN and RASER time series, with the values from the data set reconstructed with a standard magnitude calculation. This behavior once again conforms to the increase in the temporal SNR of the acquired data that was exemplified in Figure 3 showing trial averages recorded with lower R-values and processed by SR, as compared to counterparts recorded with high R-values and processed by taking the signal magnitude.

DISCUSSION

The results presented in this report demonstrate the feasibility and advantages of employing the super-resolution reconstruction algorithm for the processing of spatiotemporally-encoded fMRI data. This reconstruction approach allows one to retain the unique properties of SPEN (such as its inherent immunity to static magnetic field inhomogeneities [16]) while significantly reducing the relatively high power-deposition that was initially associated with this type of encoding. The large bandwidth pulses that were previously necessary to generate a pixel-wide point spread functions can now be avoided, as the desired spatial localization is achieved via improved post-processing reconstruction. As a result, the difference in power deposition between SPEN and EPI-based experiments targeting similar spatial resolutions is no longer significant –particularly when noticing EPI's need of additional fat-suppression pulses in order to perform a reliable Nyquist-ghost correction. SPEN-based sequences, by contrast, are not susceptible to these types of artifacts due to their higher immunity to frequency variations within the sample, and can therefore be performed without additional preparation pulses.

Another previously reported shortcoming of SPEN's magnitude calculation, was a significant SNR penalty when compared to EPI-based methods [14,16]. In many cases this penalty may not be crippling, as the statistical significance of the neuronal activation is usually hampered by temporal instabilities of physiological origin, such as heart beats and breathing, rather than by thermal noise. However, at the high spatial resolutions where thermal noise dominates over physiological noise, SPEN-based protocols that use high R-valued RF pulses and standard magnitude reconstruction produced lower t-scores than EPI counterparts due to loss in the time-series thermal SNR related to the corresponding narrower PSF. This report suggests that the SNR of SPEN images can be restored through the use of the SR reconstruction procedure. Spatial resolution and improved sensitivity are thus gained, without reducing the statistical significance of the transient signal changes induced by neuronal activation. At the same time, the immunity of SPEN based sequences to off-resonance artifacts is still retained via their ability to employ stronger imaging gradients and to their unique self T_2^* refocusing property [12,14,15].

Notwithstanding these improvements in SAR and SNR characteristics arising from the SR reconstruction, consideration should be given to the current implementation of the SPEN based protocols shown in Fig 1c–d – particularly with respect to the BOLD contrast that they entail. The same full T_2^*-refocusing property which endows these protocols with high immunity to off-resonance effects, may at the same time decrease their corresponding T_2^*-driven BOLD contrast. As previously reported in [14] the statistical significance of SPEN's lower-than-standard t-scores seems to remain valid, as this reduction is related to a lower physiological noise characterizing this type of encoding. The level of T_2^* relaxation can still be easily regulated, however, yet in a controlled way, by introducing small delays which will break the balance between the encoding and acquisition durations. Lower t-scores are hence not an intrinsic property of every form of SPEN-based imaging, as higher levels of BOLD contrast can be achieved by departing from the full T_2^* refocused regime and trading-off some of the sequences' immunity to off-resonance artifacts.

Another aspect related to the specific timing chosen for the SPEN pulse sequences, concerns the fact that strong deviations from the self-refocusing condition may not only reintroduce T_2^* relaxation effects into the signal, but also break the constant echo-time (TE) property of the RASER sequence (Fig 1d) and lead to a spatially-dependent T_2-weighting of the acquired image. As previously described, spatially-dependent T_2 weighting is inherent to the Hybrid SPEN sequence (Fig 1c), with increasing T_2-decays being associated to regions corresponding to longer TEs. This same reason will, on the other hand, endow these regions

with increased SNR levels that, according to Table 1, appear to compensate the lower T_2–weighting as the *t*-score (which are proportional to the contrast-to-noise ratio), are similar to those in the constant-TE RASER technique. Although a proper choice of parameters can be used so as to minimize the TE variation over the region-of-interest, a rigorous description of the interplay of all these timing considerations on the BOLD contrast and their effects in the context of variable TE and SNR settings, is still needed yet out of the scope of this report.

In conclusion, both the reduction in power deposition and the improvement of thermal SNR makes super-resolution the preferred processing approach for SPEN-based fMRI. Indeed, the SR-reconstruction furnishes SPEN with an additional degree of freedom in choosing the *R*-value that is often better suited to the imaging conditions at hand. The use of super-resolution can be thought of as enabling fMRI on two distinct parametric regimes: an original one that is characterized by strong encoding gradients and high RF bandwidths, and an SR-enabled one characterized by the use of lower RF bandwidths leading to relatively lower SAR and higher potential SNR. The ensuing flexibility allows one to fully utilize the unique properties of spatiotemporal-encoding, opening up new prospects of investigating brain regions that are virtually inaccessible to EPI-based techniques at 3T or higher field strengths [14]. The SR SPEN approach is particularly attractive considering the gain in T_2-contrast and in SNR at ultra-high magnetic fields where the mapping of functional activity in small anatomical structures might be realized. These and other facets of SPEN are still under investigation, and should prove important complements to the SR-derived benefits noted in the present study.

Acknowledgments

References

1. Ogawa S, Tank WD, Menon R, Ellermann MJ, Kim SG, Merkle H, Ugurbil K. Intrinsic signal changes accompanying sensory stimulation: Functional brain mapping with magnetic resonance imaging. Proc Natl Acad Sci USA. 1992; 89:5951–5955. [PubMed: 1631079]
2. Logothetis NK, Wandell BA. Interpreting the BOLD signal. Annu Rev Physiol. 2004; 66:735–69. [PubMed: 14977420]
3. Norris DG. Principles of Magnetic Resonance Assessment of Brain Function. J Magn Res Imag. 2006; 23:794–807.
4. Hu X, Huu Le T. Artifact Reduction in EPI with Phase-Encoded Reference Scan. Magn Reson Med. 1996; 36:166–171. [PubMed: 8795036]
5. Cusack R, Brett M, Osswald K. An Evaluation of the Use of Magnetic Field Maps to Undistort Echo-Planar Images. Neuro Imag. 2003; 18:127–142.
6. Liu G, Ogawa S. EPI Image Reconstruction With Correction of Distortion and Signal Losses. J Magn Res Imag. 2006; 24:683–689.
7. Pruessmann KP, Weiger M, Scheidegger MB, Boesiger P. SENSE: Sensitivity Encoding for Fast MRI. Magn Reson Med. 1999; 42:952–962. [PubMed: 10542355]
8. Griswold MA, Jakob PM, Heidemann RM, Nittka M, Jellus V, Wang J, Kiefer B, Haase A. Generalized Autocalibrating Partially Parallel Acquisitions (GRAPPA). Magn Reson Med. 2002; 47:1202–1210. [PubMed: 12111967]
9. Shrot Y, Frydman L. Spatially encoded NMR and the acquisition of 2D magnetic resonance images within a single scan. J Magn Reson. 2005; 172:179–190. [PubMed: 15649744]

10. Tal A, Frydman L. Spatial encoding and the acquisition of high definition MR images in inhomogeneous magnetic fields. J Magn Reson. 2006; 181:179–194. [PubMed: 16843690]

11. Chamberlain R, Park JY, Corum C, Yacoub E, Ugurbil K, Jack CRJ, Garwood M. RASER: a new ultrafast magnetic resonance imaging method. Magn Reson Med. 2007; 58:794–799. [PubMed: 17899612]

12. Ben-Eliezer N, Shrot Y, Frydman L. High-Definition Single-Scan 2D MRI in Inhomogeneous Fields Using Spatial Encoding Methods. Magn Reson Imag. 2010; 28:77–86.

13. Fischer, H.; Ladebeck, R. Echo-Planar Imaging Image Artifacts. In: Schmitt, F.; Stehling, MK.; Turner, R., editors. Echo-Planar Imaging - theory, technique and applications. Springer-Verlag; 1998.

14. Goerke U, Garwood M, Ugurbil K. Functional magnetic resonance imaging using RASER. NeuroImage. 2011; 54(1):350–360. [PubMed: 20699123]

15. Airaksinen AM, Niskanen JP, Huttunen JK, Nissinen J, Garwood M, Pitkanen A, Grohn O. Simultaneous fMRI and Local Field Potential Measurements During Epileptic Seizures in Medetomidine-Sedated Rats Using RASER Pulse Sequence. Magn Reson Med. 2010; 64:1191–1199. [PubMed: 20725933]

16. Ben-Eliezer N, Irani M, Frydman L. Super-Resolved Spatially-Encoded Single-Scan 2D MRI. Magn Reson Med. 2010; 63:1594–1600. [PubMed: 20512863]

17. Ben-Eliezer N, Frydman L. Spatiotemporal Encoding As A Robust Basis for Fast 3D In Vivo MRI. NMR in Biomed. 2011 (in press).

18. Park JY, Garwood M. Spin-Echo MRI Using pi/2 and pi Hyperbolic Secant Pulses. Magn Reson Med. 2009; 61:175–187. [PubMed: 19097200]

19. Kunz D. Use of frequency-modulated radiofrequency pulses in MR imaging experiments. Magn Reson Med. 1986; 3:377–384. [PubMed: 3724417]

20. Pipe JG. Spatial encoding and reconstruction in MRI with quadratic phase profiles. Magn Reson Med. 1995; 33:24–33. [PubMed: 7891532]

21. Bruder H, Fischer H, Reinfelder HE, Schmitt F. Image Reconstruction for Echo Planar Imaging with Nonequidistant k-Space Sampling. Magn Reson Med. 1990; 23:311–323. [PubMed: 1549045]

22. Strupp JP. Stimulate: A GUI based fMRI analysis software package. Neuro Imag. 1996; 3:S607.

23. Weisskoff RM. Simple Measurement of Scanner Stability for Functional NMR Imaging of Activation in the Brain. Magn Reson Med. 1996; 36:643–645. [PubMed: 8892220]

24. Duong TQ, Yacoub E, Adriany G, Hu XP, Ugurbil K, Kim SG. Microvascular BOLD contribution at 4 and 7 T in the human brain: Gradient-echo and spin-echo fMRI with suppression of blood effects. Magn Reson Med. 2003; 49:1019–1027. [PubMed: 12768579]

25. Yacoub E, Van De Moortele PF. Signal and noise characteristics of Hahn SE and GE BOLD fMRI at 7 T in humans. Neuroimage. 2005; 24:738–750. [PubMed: 15652309]

26. Jochimsen TH, Norris DG, Mildner T, Moller HE. Quantifying the Intra- and Extravascular Contributions to Spin-Echo fMRI at 3 T, Magn. Reson Med. 2004; 52:724–732.

27. Parkes LM, Schwarzbach JV, Bouts AA, Deckers RhR, Pullens P, Kerskens CM, Norris DG. Quantifying the Spatial Resolution of the Gradient Echo and Spin Echo BOLD Response at 3 Tesla. Magn Reson Med. 2005; 54:1465–1472. [PubMed: 16276507]

28. Michelich CR, Song AW, MacFall JR. Dependence of Gradient-echo and Spin-Echo BOLD fMRI at 4 T on diffusion weighting. NMR Biomed. 2006; 19:566–572. [PubMed: 16598695]

29. Goerke U, Van De Moortele PF, Ugurbil K. Enhanced relative BOLD signal changes in T2 weighted stimulated echoes. Magn Reson Med. 2007; 58:764–762.

30. Poser BA, Norris DG. Fast spin echo sequences for BOLD functional MRI. MAGMA. 2007; 20(1):11–17. [PubMed: 17245581]

31. He X, Zhu M, Yablonskiy DA. Validation of Oxygen Extraction Fraction Measurement by qBOLD Technique. Magn Reson Med. 2008; 60:882–888. [PubMed: 18816808]

32. Fujita N. Extravascular contribution of blood oxygenation level-dependent signal changes: a numerical analysis based on a vascular network model. Magn Reson Med. 2001; 46:723–734. [PubMed: 11590649]
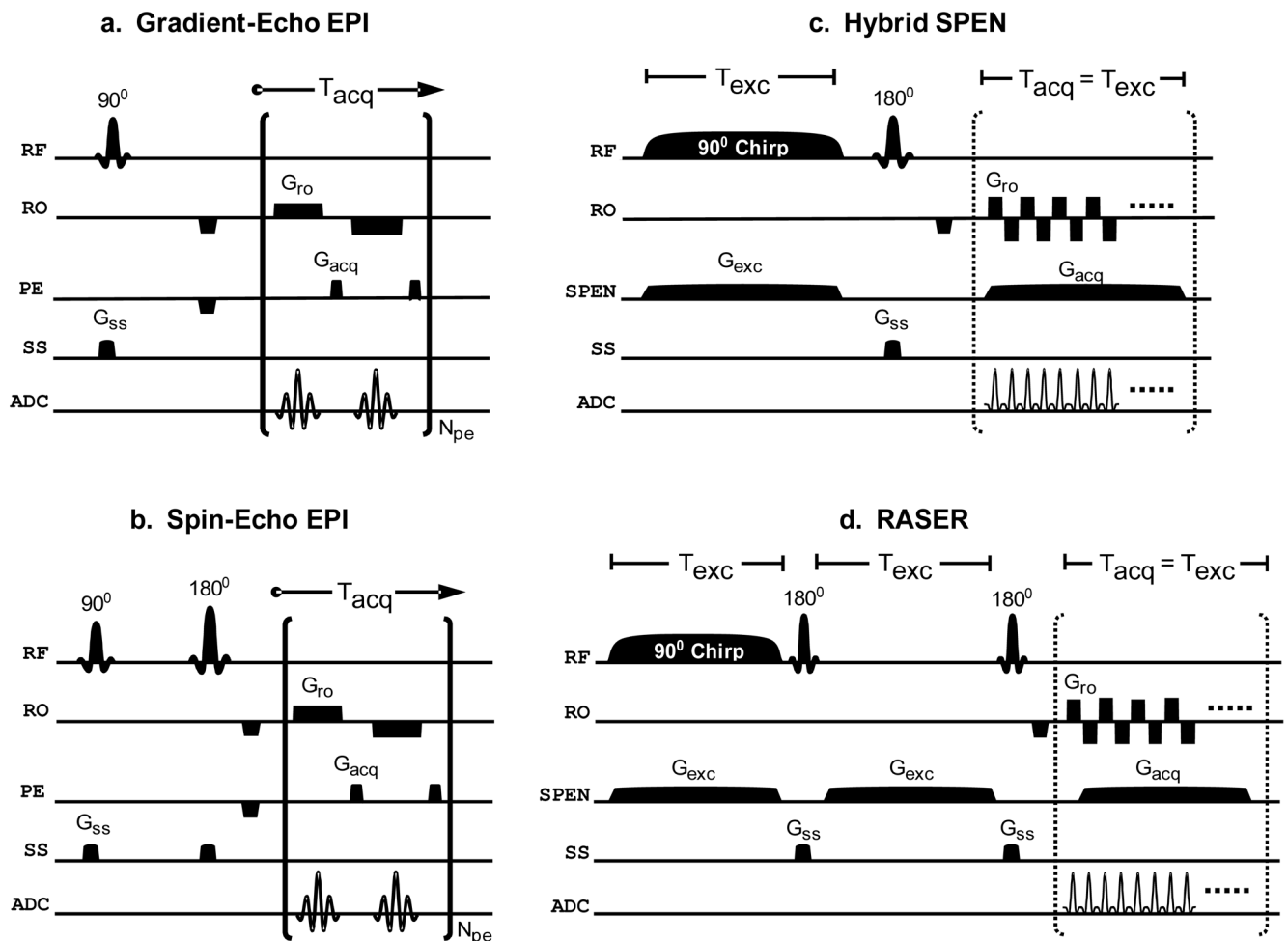
Figure 1.

Pulse sequence schemes used in the current study. (**a**) Gradient-Echo EPI (**b**) Spin-Echo EPI (**c**) Hybrid SPEN [12] (**d**) Spatiotemporally-encoded RASER [11]. In both (c) and (d) the excitation is replaced with a frequency-swept pulse, while slice-selection is performed using 180° selective pulses. Abbreviations denote: *exc* excitation, *acq* acquisition, *RF* irradiation channel, *RO* readout channel, *PE/SPEN* phase- or SPEN-encoded channel, *SS* slice-selection channel, *ADC* signal acquisition channel, N_{pe} number of phase/spatiotemporally-encoded lines.
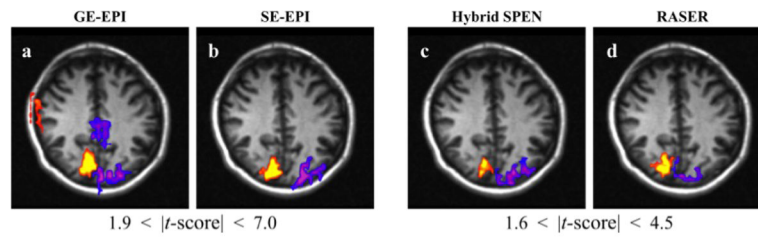
Figure 2.
Comparison between the fMRI maps (colored) arising from alternating left & right visual stimuli, based on the four different sequence schemes given in Figure 1. The positive *t*-scores (yellow) represent stimulation of the left visual hemifield, while the negative values (purple) correspond to right visual hemifield stimulation. fMRI responses are given for one representative subject out of the four tested, and are shown overlaid on top of a corresponding multi-scan T_1-weighted high-resolution FLASH image [ROI = 192×192 mm]. (**a**) Gradient-Echo EPI (**b**) Spin-Echo EPI (**c**) Hybrid SPEN [12] (**d**) Spatiotemporally-encoded RASER [11].

High _R_-value   **Low _R_-value**

without SR   without SR   with SR

Single-shot Functional images

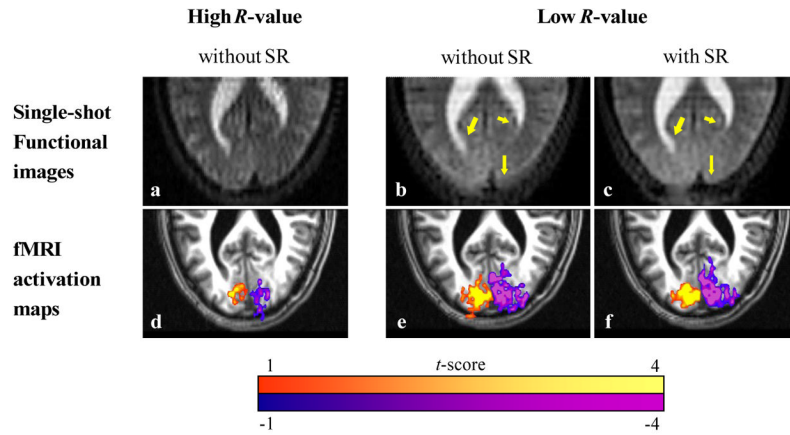fMRI activation maps

1   _t_-score   4

-1   -4

Figure 3.
Assessment of the SR reconstruction procedure applied to, **Top:** single T$_2$-weighted functional images, and **Bottom:** fMRI time series of alternating left & right visual stimuli, corresponding respectively to positive (yellow) and to negative (purple) _t_-values. Maps are shown for one representative subject out of the three tested, and are displayed (lower row) overlaid on a corresponding T$_1$-weighted high-resolution FLASH image [ROI = 192×96 mm]. All data were collected using the Hybrid SPEN sequence shown in Figure 1c. Left column (**a,d**): data acquired using high _R_-values having an optimal _a priori_ resolution (_i.e.,_ one voxel per sampled point along the SPEN axis). Middle column (**b,e**): data acquired using low _R_-values and reconstructed with magnitude-only algorithm. In this case, spatial resolution is reduced due to the broader PSF and blurring is observed in both the T$_2$-weighted image and the activation map. Right column (**c,f**): images acquired using low _R_-values and super-resolved in post-processing. Yellow arrows mark regions highlighting the resolution enhancement afforded by the SR procedure.
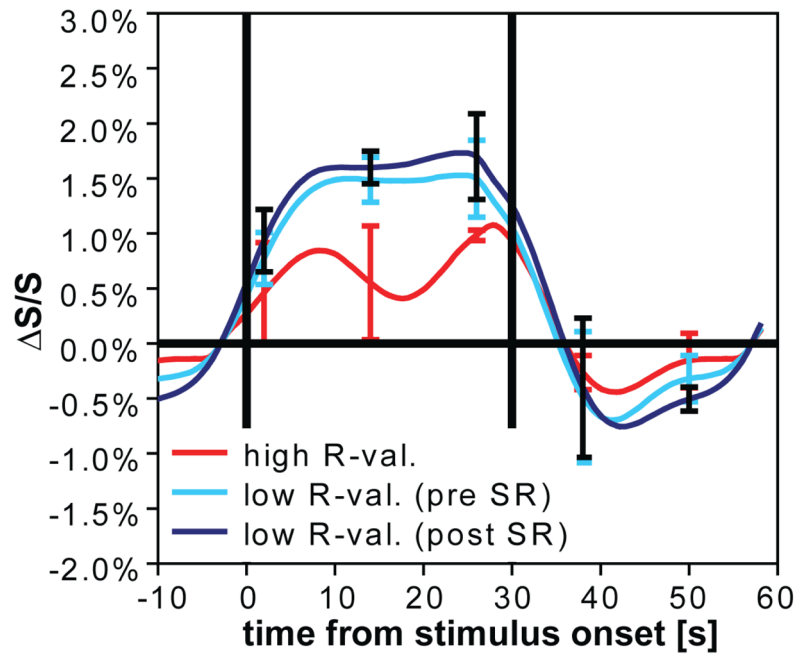
Figure 4.

Figure 4 *(color)*: Trial averages of the mean time courses within a region of interest during visual stimuli fMRI experiments. The curves represent the mean of data sets of three subjects; error bars (displayed for some data points) represent the standard deviation of the variation between subjects. **Red:** Data derived from time courses acquired with the Hybrid SPEN sequence shown in Figure 1c using standard resolution, that is, high *R*-value; **Cyan:** time courses acquired using a low *R*-value prior to applying super-resolution reconstruction, and **Black:** the same time courses after applying super-resolution reconstruction. The vertical black lines mark onset (0 s) and end (30 s) of visual stimulation. The results from the left and right visual hemifield stimulations have been merged.

Table 1

Mean *t*-score, number of activated voxels, and thermal SNR in a selected ROI of the visual cortex, for Hybrid SPEN and RASER time series reconstructed at standard resolution (high *R*-value) and for a time series acquired with low *R*-value before and after super-resolution reconstruction. Mean *t*-score values were calculated by combining the *t*-scores from the left and right visual hemifield stimulations (absolute values), and represent an average across the three subjects. Numbers in round brackets indicate the standard deviation resulting from inter-subject variability.

		Mean *t*-score	Number of activated voxels	SNR
Hybrid SPEN	High *R*-value	0.4 (0.2)	113 (9)	80 (14)
	Low *R*-value (pre SR)	1.3 (0.2)	140 (24)	310 (10)
	Low *R*-value (post SR)	1.3 (0.3)	140 (13)	300 (20)
RASER	High *R*-value	0.36 (0.06)	90 (4)	75 (2)
	Low *R*-value (pre SR)	0.66 (0.06)	120 (30)	250 (40)
	Low *R*-value (post SR)	0.8 (0.1)	130 (50)	250 (60)